

Montmorillonite-surfactant hybrid particles for modulating intestinal P-glycoprotein-mediated transport

Nielsen, Rasmus Blaaholm; Kahnt, Ariane; Dillen, Lieve; Wuyts, Koen; Snoeys, Jan; Nielsen, Ulla Gro; Holm, René; Nielsen, Carsten Uhd

Published in:
International Journal of Pharmaceutics

DOI:
[10.1016/j.ijpharm.2019.118696](https://doi.org/10.1016/j.ijpharm.2019.118696)

Publication date:
2019

Document Version
Peer reviewed version

Citation for published version (APA):
Nielsen, R. B., Kahnt, A., Dillen, L., Wuyts, K., Snoeys, J., Nielsen, U. G., Holm, R., & Nielsen, C. U. (2019). Montmorillonite-surfactant hybrid particles for modulating intestinal P-glycoprotein-mediated transport. *International Journal of Pharmaceutics*, 571, [118696]. <https://doi.org/10.1016/j.ijpharm.2019.118696>

General rights

Copyright and moral rights for the publications made accessible in the public portal are retained by the authors and/or other copyright owners and it is a condition of accessing publications that users recognise and abide by the legal requirements associated with these rights.

- Users may download and print one copy of any publication from the public portal for the purpose of private study or research.
- You may not further distribute the material or use it for any profit-making activity or commercial gain.
- You may freely distribute the URL identifying the publication in the public portal.

Take down policy

If you believe that this document breaches copyright please contact rucforsk@kb.dk providing details, and we will remove access to the work immediately and investigate your claim.

**Montmorillonite-surfactant hybrid particles for modulating
intestinal P-glycoprotein-mediated transport**

Rasmus Blaaholm Nielsen¹, Ariane Kahnt², Lieve Dillen², Koen Wuyts², Jan Snoeys², Ulla Gro Nielsen¹, René Holm^{3, 4}, Carsten Uhd Nielsen^{1*}

¹Department of Physics, Chemistry and Pharmacy, University of Southern Denmark, Campusvej 55, DK-5230 Odense M, Denmark

²Drug Metabolism and Pharmacokinetics, Janssen R&D, Johnson & Johnson, Turnhoutseweg 30, BE-2340 Beerse, Belgium

³Drug Product Development, Janssen R&D, Johnson & Johnson, Turnhoutseweg 30, BE-2340 Beerse, Belgium

⁴Department of Science and Environment, Roskilde University, Universitetsvej 1, DK-4000 Roskilde, Denmark

*Corresponding author at: Department of Physics, Chemistry and Pharmacy, University of Southern Denmark, Campusvej 55, DK-5230 Odense M, Denmark, phone: +45 6550 9427, e-mail: cun@sdu.dk

Running title: MSH Particles increase digoxin exposure

17 **Abstract**

18 In the small intestine, P-glycoprotein (P-gp) may limit the permeability of its substrates, which lead
19 to reduced oral absorption. To circumvent the effect of P-gp, a nanocomposite material termed
20 *montmorillonite-surfactant hybrid particles* was developed. The particles consisted of
21 montmorillonite, the P-gp-inhibiting, nonionic surfactant, polysorbate 20, and the P-gp substrate,
22 digoxin. The present study aimed to investigate if montmorillonite-surfactant hybrid particles could
23 modulate the absorption of digoxin *in vivo*. Montmorillonite-surfactant hybrid particles were prepared
24 by lyophilising an aqueous suspension of the constituents. Scanning electron microscopy (SEM),
25 thermogravimetric analysis (TGA), and powder X-ray diffraction (PXRD) revealed an altered surface
26 morphology, decreased water content, and intercalation of polysorbate 20 between montmorillonite
27 layers. The particles were administered orally to Sprague Dawley rats, and digoxin was quantified by
28 liquid chromatography-tandem mass spectrometry. Control digoxin-containing montmorillonite
29 decreased the exposure of digoxin. In contrast, montmorillonite-surfactant hybrid particles increased
30 AUC and C_{max} by 31 and 91 %, respectively, compared to digoxin in solution. It was hypothesised
31 that montmorillonite-surfactant hybrid particles increased digoxin exposure by forming mucosa-
32 localised elevated concentrations of polysorbate 20 and digoxin, which enhanced the inhibitory effect
33 of polysorbate 20 on P-gp.

34 **Keywords:** Intestinal absorption, montmorillonite, nanocomposites, digoxin, P-glycoprotein,
35 polysorbate 20

36 **Abbreviations:** FWHM, the full width at half maximum; LBF, lipid-based formulation; MSH,
37 montmorillonite-surfactant hybrid, P-gp, P-glycoprotein; SPE, solid phase extraction.

38 **List of compounds studied:** Polysorbate 20, montmorillonite, digoxin.

39 **1 Introduction**

40 Pharmacokinetic properties of drug substances have gained increased focus in early drug
41 development, as an estimated 10-20 % of drug candidates fail in preclinical development or in clinical
42 trials, because of undesirable pharmacokinetic properties (Cook et al., 2014; Di and Kerns, 2016;
43 Kola and Landis, 2004). These undesirable pharmacokinetic properties are often caused by
44 P-glycoprotein (P-gp) (Di and Kerns, 2016), which is a widely expressed efflux transporter (Thiebaut
45 et al., 1987). In the apical membrane of the intestinal epithelium, P-gp mediates cellular efflux of
46 numerous drug substances, which leads to decreased absorption and bioavailability of the drug
47 substance in question (Leslie et al., 2005; Lin and Yamazaki, 2003).

48 Numerous nonionic surfactants have been shown to inhibit P-gp in cell- and animal models, albeit in
49 relatively high concentrations (Al-Ali et al., 2019; Cornaire et al., 2004; Lo, 2003; Zhang et al., 2003).
50 Polysorbate 20 is among the most potent surfactant-based P-gp inhibitors investigated (Al-Ali et al.,
51 2018a; Al-Ali et al., 2018b; Al-Saraf et al., 2016; Gurjar et al., 2018; Lo, 2003). Co-administration
52 of 0.55 g kg⁻¹ polysorbate 20 significantly increased the oral bioavailability of the P-gp substrate,
53 digoxin, in rats from 59 to 84 %, and increased C_{max} by 79 % (Nielsen et al., 2016). Corresponding
54 administration of digoxin to *mdr1a* knockout rats produced an increased bioavailability, and there
55 was no effect of co-administration of polysorbate 20 (Nielsen et al., 2016). This suggested that
56 solubilising effects and/or increased passive permeability were not the cause of the increased
57 absorption in wild type rats. However, a polysorbate 20 dose of 0.55 g kg⁻¹ corresponds to a dose of
58 approximately 6 g in humans, when a simple proportional weight scaling is applied (Nair and Jacob,
59 2016), i.e., more than thrice that of the WHO-recommended maximal daily dose of 25 mg kg⁻¹
60 (Sheskey et al., 2017). Thus, there is a need to potentiate the effects of polysorbate 20 on P-gp to
61 develop an applicable polysorbate 20-based formulation for intestinal P-gp inhibition.

62 *In vitro*, only 200 μM (246 $\mu\text{g mL}^{-1}$) polysorbate 20 was required to completely inhibit P-gp-mediated
63 digoxin efflux in Caco-2 cells (Nielsen et al., 2016). Meanwhile, 10 % v/v (110 mg mL^{-1}) polysorbate
64 20 in the dosing solution was necessary to produce the highest observed inhibition of intestinal P-gp
65 activity, *in vivo* (Nielsen et al., 2016). This 450-fold difference could be related to the fact that the *in*
66 *vitro* transport system is stationary, while the intestinal lumen is a dynamic system with intestinal
67 dilution, intestinal transit, and a redundancy in the area able to mediate absorption. Therefore, a
68 formulation approach may be applied, in which polysorbate 20 and digoxin are released in the vicinity
69 of the epithelial cells to modify the absorption process. We hypothesise that the clay nanomaterial,
70 montmorillonite, can be applied as a drug substance- and excipient carrier in this context.

71 Montmorillonite has previously been investigated as a drug carrier (Aguzzi et al., 2007; Ruiz-Hitzky
72 et al., 2010). Montmorillonite, like other clays, has a distinct layered structure and surface chemistry,
73 and montmorillonite elicits a strong ability to retain cations (Hensen and Smit, 2002). Countless
74 complex possibilities exist when montmorillonite is combined with for example polymers,
75 surfactants, and dyes to form nanocomposites. Many potential applications have been investigated
76 from wound dressings to food packaging and waste water treatment (Kokabi et al., 2007; Rhim et al.,
77 2013; Wang and Wang, 2007). However, the application of montmorillonite-based nanocomposites
78 has received limited attention in the pharmaceutical field. The most common approach has been to
79 intercalate cationic drug substances between montmorillonite layers to obtain either a modulated drug
80 release or a solubilising effect on the drug substance in question (Aguzzi et al., 2007). Neutral drug
81 substances have also been shown to adsorb to montmorillonite surfaces via ion-dipole interactions
82 (Su and Carstensen, 1972), and montmorillonite has been recognised as a possible solid carrier for
83 lipid-based formulations (LBF) (Denning et al., 2017; Denning et al., 2018; Feeney et al., 2016).
84 Calabrese and co-workers have successfully incorporated polysorbate 20 in montmorillonite to obtain
85 delayed release of cinnamic acid (Calabrese et al., 2016; Calabrese et al., 2017), and they showed that

polysorbate 20 facilitated the release of cinnamic acid from montmorillonite. Their studies also confirm the strong interactions between montmorillonite and polymers or surfactants that contain oxyethylene groups (-CH₂-CH₂-O-), like polysorbate 20 (Aranda and Ruiz-Hitzky, 1992). Additionally, it has been shown that montmorillonite has mucoadhesive properties. For example, it was shown that montmorillonite intercalated with tetracycline displayed mucoadhesive forces to porcine mucus corresponding to 43 % of chitosan, which is a known highly mucoadhesive polysaccharide (Iannuccelli et al., 2015). As a result, studies have focused on montmorillonite and composites hereof to obtain mucoadhesive drug delivery systems for gastroretention or local oral administration (Aguzzi et al., 2007; Calabrese et al., 2013; Iannuccelli et al., 2015; Onnainty et al., 2016).

Montmorillonite or other clay-based nanomaterials have not been investigated in pharmaceutical science to obtain modulation of intestinal drug transporters, to our knowledge. Based on literature findings that montmorillonite has mucoadhesive properties and displays modified drug substance release in combination with polysorbate 20, we hypothesise that montmorillonite-surfactant hybrid (MSH) particles intercalated with polysorbate 20 and digoxin may lead to increased exposure of digoxin, compared to corresponding doses of polysorbate 20 and digoxin in simple solutions. The present study aimed to prepare and characterise MSH particles and to assess the pharmacokinetics of digoxin in rats after administration as MSH particles, compared to administration as simple solutions containing polysorbate 20.

2 Materials and methods

2.1 Materials

Digoxin, triple deuterated (D₃)-digoxin, polysorbate 20, bovine serum albumin (albumin fraction V) > 97 %, montmorillonite as ‘nanoclay, hydrophilic bentonite’, and all other chemicals in analytical grade quality or higher were from Merck KGaA (Germany). Ultrapure water was obtained from an

110 in-house Milli-Q purification system (Millipore, MA, USA). Blank rat plasma was from
111 Bioreclamation IVT (NY, USA).

112 2.2 Preparation of montmorillonite-surfactant hybrid particles

113 MSH particles were prepared with a fixed 1:1 w/w ratio of montmorillonite and polysorbate 20 along
114 with an amount of digoxin that allowed a constant digoxin dose and variable doses of montmorillonite
115 and polysorbate 20 (Table 1). Furthermore, two control formulations were prepared. One contained
116 montmorillonite and digoxin, designated *digoxin-containing montmorillonite*, and one contained only
117 montmorillonite, designated *lyophilised montmorillonite*.

118 Suspensions of montmorillonite, polysorbate 20, and digoxin were obtained by suspending
119 montmorillonite in 11.0 mL ultrapure water (Milli-Q) in a beaker fitted with a magnet and stirred for
120 4 h. The pH was 9.5 after hydration of the montmorillonite suspension, and the pH was subsequently
121 adjusted to 7.0 ± 0.1 with HCl. In parallel, polysorbate 20 was added to a screwcap vial together with
122 1000 μL of a 1.00 mg mL^{-1} digoxin stock solution in 96 % v/v ethanol. The mixture was ultrasonicated
123 for 30 min to ensure solubilisation of digoxin using an Elmasonic P30H ultrasonic bath (Elma
124 Schmidbauer, Germany). 12.0 mL of ultrapure water was then added, and the polysorbate 20-digoxin
125 mixture was ultrasonicated for 60 min to aid micelle formation. Then, the polysorbate 20-digoxin
126 solution was added to the montmorillonite suspension dropwise (5 min), and the resulting suspension
127 was stirred for 24 h with the pH maintained at 7.5 ± 0.5 by manual addition of microvolumes of 1 M
128 HCl. The suspension was divided into ten separate 10 mL lyophilisation vials and stored at -20°C
129 overnight. The frozen suspensions were lyophilised in a Beta 2-8 LSCBasic table top freeze dryer
130 (Martin Christ, Germany). Main drying lasted for 40 h, applying a system pressure of 0.200 mbar, a
131 shelf temperature of -25°C , and a condenser temperature of approximately -85°C . The final drying
132 lasted for 4 h, applying a system pressure of 0.011 mbar, a shelf temperature of 25°C , and a condenser
133 temperature of approximately -85°C . Following lyophilisation, the chamber was filled with dry N_2

134 gas, and the vials were quickly equipped with rubber stoppers. The total MSH particle content in each
135 vial was assessed by weighing the vial before filling and after lyophilisation. The products appeared
136 either as cakes or powders depending on the concentration of montmorillonite in the final suspensions
137 with increasing montmorillonite amounts resulting in a stable cake.

138 2.3 Characterisation of MSH particles

139 The MSH particles were characterised by scanning electron microscopy (SEM), thermogravimetric
140 analysis (TGA), and powder X-ray diffraction (PXRD).

141 2.3.1 Scanning electron microscopy

142 SEM was carried out with a Phenom ProX scanning electron microscope (Thermo Fisher Scientific,
143 MA, USA). A small amount of powder was mounted on 12 mm stubs with carbon tabs (Agar
144 Scientific, UK) and coated with gold by a Q150S rotary-pumped sputter coater-carbon coater
145 (Quorum, UK). Imaging was carried out at an accelerating voltage of 5 kV at magnifications
146 $\times 175$ -2900 and 10 kV at magnifications $\times 4300$ -29000.

147 2.3.2 Thermogravimetric analysis

148 TGA was carried out on a Q500 thermogravimetric analyser (TA Instruments, TX, USA). Samples
149 of 2-4 mg was equilibrated at 30 °C for 2 min before the temperature was increased to 700 °C at a
150 rate of 10 °C min⁻¹.

151 2.3.3 Powder X-ray diffraction

152 PXRD was carried out with a PANalytical X'pert PRO multipurpose diffractometer (Malvern
153 Panalytical, UK). Scanning was performed with a Cu K α , $\lambda = 1.5406$ Å radiation source in the 2 θ
154 range from 3 to 50 ° with a scan speed of 0.254 ° s⁻¹ and a step size of 0.0167 °. The voltage and
155 current were set to 45 kV and 40 mA, respectively. Samples were prepared on 16 mm zero
156 background plates.

157 Miller indices were applied to describe the lattice planes in a sample that caused the observed
158 reflections in powder X-ray diffractograms. A lattice plane can be described by three integers (hkl),
159 and the main interest of the present study was the (001) reflection, which is the reflection
160 corresponding to the distance between two individual montmorillonite layers. Reflections caused by
161 lattice planes within the individual montmorillonite layers, which were not related to interlayer
162 distance, can be described as ($hk0$) reflections. The interlayer spacing of montmorillonite was
163 calculated from the diffraction angles at maximum intensity of (001) reflections using Bragg's law:

$$n \lambda = 2d \sin(\theta) \quad (I)$$

164 where n is the number of wavelengths, λ is the wavelength of the X-ray source, d is the interlayer
165 spacing, and θ is the diffraction angle. Reflections were assigned by a comparison with literature
166 (Viani et al., 2002). The full width at half maximum (FWHM) was estimated by manual readouts.

167 2.4 In vivo study

168 The study was carried out in accordance with European and Belgian law controlling the experiments
169 on animals. 60 male Sprague Dawley rats (10 groups, $n=6$) were supplied from Charles River (MA,
170 USA) and acclimatised 11-12 days before conductance of the study. At the beginning of the study,
171 the animals weighed 245-300 g (approximately 9 weeks of age) and were fasted for about 16 h prior
172 to the experiment.

173 Animals were dosed by oral gavage with 5 mL kg^{-1} solutions or suspensions containing 0.02 mg kg^{-1}
174 digoxin in 40 % v/v ethanol in water. Dosing overview of the individual groups is shown in Table 2.
175 The amount of ethanol administered did not affect the rats' clinical behaviour.

176 Blood samples were taken 15, 30, 45, 60, 120, 180, 240, and 360 min after administration. Micro
177 sampling was performed by placing the rats in a restrainer and puncturing the tail vein with a 25G
178 needle. 64 μL of blood was then collected in a glass capillary (Vitrex Medical, Denmark) and closed

179 in one end with a sigillum wax plate (Vitrex Medical, Denmark). Capillaries containing blood
180 samples were placed in centrifuge tubes and kept on ice until centrifugation (1900 G, 4 °C, 10 min).
181 After centrifugation, the clear part of the capillary, containing plasma, was cut off, and the plasma
182 was transferred to two 10 µL end-to-end pipettes (Vitrex Medical, Denmark) and placed in two
183 individually labelled 1 mL Fluid X tubes (Brooks Life Sciences, MA, USA) with lids and stored in a
184 96-well format. Samples were kept at -20 °C until analysis. The rats were euthanised after the last
185 blood sample.

186 2.4.1 Bioanalysis

187 Calibration standards of digoxin were prepared in rat plasma to obtain concentrations of
188 2-100 ng mL⁻¹. Quality control samples of 8, 50, and 100 ng mL⁻¹ solutions were prepared by spiking
189 rat plasma with appropriate amounts of digoxin stock solution. Calibration standards and quality
190 control samples were stored in 10 µL end-to-end pipettes placed in Fluid X tubes and kept in a freezer
191 (-20 °C) until sample preparation and were treated like the plasma samples as described below.

192 To wash out sample plasma from the end-to-end pipettes, 100 µL 2 % w/v bovine serum albumin in
193 phosphate buffer (pH 7.5) was added to the sample tubes, and the samples were shaken horizontally
194 (10 min, 500 min⁻¹) and subsequently centrifuged (5 min, 20 °C, 2300 × g). A 55 µL aliquot of the
195 sample was then transferred to a new Fluid X tube, and 55 µL internal standard (25 ng mL⁻¹ D₃-
196 digoxin in methanol) was added. The pH of the resulting mixture was adjusted to 9 by addition of 25
197 µL of a 2 M ammonium acetate solution followed by dilution with 175 µL Milli-Q purified water.
198 The samples were shaken by vortex mixing after each addition.

199 Oasis® HLB 96 well solid phase extraction (SPE) plates, 30 µm particle size, 30 mg sorbent per well
200 (Waters, MA, USA) were conditioned with 1 mL methanol, 1 mL Milli-Q purified water, and 3 × 0.5
201 mL 0.1 M ammonium acetate (pH 9). Positive pressure (~ 3 psi) was applied after each addition, until

the resin was dry. Subsequently, the entire sample volume (310 μL) was transferred to the conditioned SPE well plates and positive pressure (~ 1.5 psi) was applied to load the samples slowly. The SPE wells were then washed with 3×0.5 mL 0.1 M ammonium acetate (pH 9). A positive pressure (~ 3 psi) was applied after each addition, until the resin was dry. The samples were then eluted from the SPE resin with 2×0.5 mL and 1×0.2 mL ethanol into a new 96-well plate. The eluent was then dried under a 40 L min^{-1} flow of dry N_2 at room temperature (Porvair Minivap, Porvair Sciences, UK) and reconstituted in 300 μL 1:1 methanol:water mixture followed by vortex mixing. After a centrifugation step (10 min, $6000 \times g$) the samples were transferred to a round 96-well plate for chromatographic analysis.

Liquid chromatography-tandem mass spectrometry (LC-MS/MS) analysis was carried out on a 6500 Sciex triple quad instrument (ABSciex, Canada), which was coupled to a UHPLC-system (Shimadzu, Japan). The chromatographic separation was carried out using a reversed phase UPLC column (Acquity BEH C18, $1.7 \mu\text{m}$, 50×2.1 mm, Waters, MA, USA). The mobile phases consisted of 0.01 M ammonium carbonate (solvent A) and methanol (solvent B), and a gradient elution at 45°C was performed (starting at 50 % solvent A, 50 % solvent B to 75 % solvent B in 2.3 min, followed by isocratic hold at 95 % B for 1.19 min and re-equilibration to 50 % B in 0.99 min). Total run time was 4.5 min and a flow rate of 0.3 mL min^{-1} was applied.

The LC-MS/MS was operated in positive ion mode using the TurboIonSprayTM-interface (electrospray ionisation), and was optimised for the quantification of digoxin, applying multiple reaction monitoring (m/z 798.6 \rightarrow m/z 651).

The calibration curve ranged from 2-100 ng mL^{-1} and linear regression with a weighing factor of $1/x^2$ was used to produce the best fit for the concentration-detector response relationship. The lower limit of quantification was 2 ng mL^{-1} . The accuracy of all batches, as measured by independent quality

control samples, were between 80-120 % of the nominal value over the entire range for the plasma samples.

2.4.2 Data analysis

The AUC of digoxin in the pharmacokinetic profile in the range 0-6 h was calculated by the trapezoidal method. First order elimination was assumed, and the elimination rate constant (k_e) of digoxin was estimated by performing linear regression of \ln to the plasma concentrations as a function of time using data points at 2, 3, 4, and 6 h. The slope of the resulting regression was $-k_e$. R^2 values were generally above 0.90. Plasma profiles were also fitted to zero order elimination with a simple linear regression for the time points stated above. All formulations, except digoxin-containing montmorillonite, displayed a higher R^2 of the fit with first order elimination. It was assumed that the formulations did not affect elimination, and that the difference observed for digoxin-containing montmorillonite was caused by prolongation of absorption into the elimination phase, rather than altered elimination. For this reason, plasma profiles for the treatment with digoxin-containing montmorillonite was still analysed as first order elimination.

The $t_{1/2}$ of digoxin was calculated:

$$t_{1/2} = \frac{\ln(2)}{k_e} \quad (\text{II})$$

Each analysis of AUC_{0-6h} and elimination was performed for each individual data set, before statistical analysis.

2.4.3 Statistical analysis

Statistical analysis was performed in GraphPad Prism 8.1.2. The pharmacokinetic parameters, AUC_{0-6h} , C_{\max} , the plasma concentration at the first sampling point ($C_{15 \text{ min}}$), and $t_{1/2}$ of each group of animals were compared by one-way ANOVA, followed by a Dunnett's test in the following order: Co-administration of the three doses of polysorbate 20 was compared to digoxin administered alone,

247 and administration of MSH particles A-E was compared to both digoxin administered alone and to
248 digoxin-containing montmorillonite in two separate analyses. A student's t test was applied to
249 compare the pharmacokinetic parameters after administration of digoxin-containing montmorillonite
250 and digoxin only. All P-values below 0.05 were considered statistically significant.

251 **3 Results**

252 *3.1 Characterisation of MSH particles*

253 The untreated montmorillonite was light-brown or beige, as was the lyophilised- and digoxin-
254 containing montmorillonite formulations without polysorbate 20. In contrast, polysorbate 20-
255 containing MSH particle formulations were more pale and had an off-white colour.

256 *3.1.1 Scanning electron microscopy*

257 The shape and surface morphology of the montmorillonite particles was investigated by SEM.
258 Untreated montmorillonite (Fig. 1A) contained pores of irregular shape with the observed perimeter
259 diameters in the range 0.8-2.5 μm . The surface morphology of digoxin-containing (Fig. 1B) and
260 lyophilised montmorillonite (Fig. S2B) appeared similar on the SEM images. Comparison of the SEM
261 images of untreated montmorillonite with lyophilised montmorillonite and digoxin-containing
262 montmorillonite, showed that lyophilisation resulted in a more porous structure with pore diameters
263 of 0.5-3 μm , which was also observed when polysorbate 20 was intercalated (Fig. 1C and D).
264 Additionally, when polysorbate 20 was intercalated, the pores and the appearance of the particle
265 surface for MSH particles changed to smoother and more circle- or ellipse-shaped pores, as compared
266 to digoxin-containing and lyophilised montmorillonite.

267 The particle shape changed from spheres to irregular particles with sharp edges upon lyophilisation
268 (Fig. S1). The observed perimeter diameter of the untreated montmorillonite particles was in the range
269 of 4-50 μm . The irregular MSH particles and digoxin-containing montmorillonite was in the range of
270 2-200 μm , while lyophilised montmorillonite was in the range of 2-500 μm (Fig. S2A).

271 3.1.2 Thermogravimetric analysis

272 The composition and stability of the starting compounds and the prepared formulations were assessed
273 by TGA (Fig. 2). The characteristic temperature intervals and corresponding thermogravimetric mass
274 loss are given in Table S1. Untreated montmorillonite contained 11 % physically adsorbed water and
275 4 % interlayer water. Dehydroxylation of the untreated montmorillonite accounted for a 3 % mass
276 loss, resulting in a mass of 83 % left in the pan after heating to 700 °C (residual mass). Polysorbate 20
277 contained 2 % water and 96 % mass was lost during degradation, which left a residual mass of 1 %.

278 Lyophilised and digoxin-containing montmorillonite contained less physically adsorbed water than
279 untreated montmorillonite with 5 and 7 %, respectively, and 4 % interlayer water. Furthermore,
280 lyophilised and untreated montmorillonite displayed an 87 % and 86 % residual mass, respectively
281 (Table S1). These residuals correspond to untreated montmorillonite, when corrected for water
282 content.

283 MSH particles displayed an even lower content of both physically adsorbed water at 1 % and
284 interlayer water at 1 %. Degradation of polysorbate 20 led to a 53 % mass loss, and montmorillonite
285 dehydroxylation accounted for 1 % mass loss, which resulted in a 45 % residual, corresponding to
286 montmorillonite content. Additionally, comparison of polysorbate 20 and MSH particles showed that
287 polysorbate 20 decomposed at a lower temperature, when it was incorporated into MSH particles as
288 the polysorbate 20 degradation was shifted approximately 35 °C down.

289 3.1.3 Powder X-ray diffraction

290 The interlayer spacing of montmorillonite in the MSH particles was investigated by PXRD, as shown
291 in Fig. 3. The interlayer spacing, which was determined from the (001) reflection was 14.9 Å in
292 untreated montmorillonite and increased to 18.0 Å in MSH particles. The (001) reflection for
293 untreated montmorillonite displayed a FWHM of 1.66 °, while the (001) reflection of MSH particles

294 was narrower with a FWHM of 1.00 °. Additionally, the (002), (003), (005), and (006) reflections
295 were present in the MSH particle diffractogram, but not in the untreated montmorillonite
296 diffractogram. For both digoxin-containing montmorillonite and lyophilised montmorillonite, none
297 of the (00 l) reflections were observed (Fig. 3).

298 At larger diffraction angles, all formulations showed reflections at approximately 20, 35, and 40 °.
299 They can all be assigned to ($hk0$) reflections or combinations including these, which were all
300 independent of the orientation of the individual montmorillonite layers. Reflections at 29 ° were only
301 present for untreated montmorillonite, digoxin-containing montmorillonite, and lyophilised
302 montmorillonite.

303 3.2 *In vivo* study

304 The pharmacokinetics of digoxin was investigated in male Sprague Dawley rats, when polysorbate 20
305 was co-administered in simple solutions and in MSH particles. The pharmacokinetic profiles are
306 shown in Fig. 4, while obtained pharmacokinetic parameters are summarised in Table 3. The effects
307 of the applied formulations were most notable on C_{\max} and $C_{15 \text{ min}}$. Overall, the plasma concentration
308 of digoxin reached a maximum within the first 45 min (Table 3). Elimination generally followed first
309 order kinetics and there was no apparent correlation between formulation type and $t_{1/2}$ (Table 3).

310 Formulations that contained polysorbate 20 in simple solutions did not alter AUC_{0-6h} . However, they
311 tended to decrease t_{\max} and increase C_{\max} and $C_{15 \text{ min}}$ of digoxin (Fig. 4A). $C_{15 \text{ min}}$ was increased in a
312 statistically significant manner for co-administration of 55 and 274 mg kg^{-1} polysorbate 20 (Table 3).

313 When digoxin was administered as digoxin-containing montmorillonite, a great alteration of the
314 pharmacokinetic profile was observed (Fig. 4B). Administration of digoxin-containing
315 montmorillonite resulted in significantly lowered AUC_{0-6h} , C_{\max} and $C_{15 \text{ min}}$, compared to digoxin only
316 (Table 3), and C_{\max}/t_{\max} could not clearly be defined (Fig. 4B).

317 In contrast, when digoxin was administered as MSH particles, containing montmorillonite *and*
318 polysorbate 20, AUC_{0-6h} , C_{max} , and $C_{15\ min}$ all increased 2-4-fold, compared to digoxin-containing
319 montmorillonite (Table 3). For doses of 137-548 mg kg⁻¹ montmorillonite and polysorbate 20, these
320 increases were statistically significant. In concordance, the incorporation of polysorbate 20 also led
321 to decreased t_{max} (Table 3). Compared to digoxin administered alone, MSH particles increased
322 AUC_{0-6h} , C_{max} and $C_{15\ min}$, and the increase in C_{max} and $C_{15\ min}$ for the 548 mg kg⁻¹ MSH formulation
323 was statistically significant (Table 3).

324 In some cases, MSH particles also tended to increase both AUC_{0-6h} and C_{max} of digoxin, compared to
325 co-administration of polysorbate 20 in simple solutions in the corresponding doses. For example, co-
326 administration of 548 mg kg⁻¹ polysorbate 20 as MSH particles increased AUC_{0-6h} and C_{max} of digoxin
327 31 % and 32 %, compared to co-administration of 548 mg kg⁻¹ polysorbate 20 in a simple solution
328 (Fig. 4D).

329 **4 Discussion**

330 *4.1 Polysorbate 20 is intercalated in MSH particles*

331 The obtained MSH particles were solid, even though they consisted of 52 % polysorbate 20, which
332 is liquid at room temperature. This phase transition may occur, because polysorbate 20 was adsorbed
333 to the montmorillonite surfaces. This was supported by the lighter colour of the MSH particles, which
334 indicated that polysorbate 20 coated the montmorillonite surface, as also reflected by the particle
335 morphology according to SEM. Lyophilised montmorillonite, digoxin-containing montmorillonite,
336 and MSH particles were subjected to the same lyophilisation cycle, but the total water content was
337 considerably lower in MSH particles. The lower interlayer water content suggested that the
338 intercalation of polysorbate 20 led to extrusion of water from the interlayer spaces. The destabilisation
339 of polysorbate 20, when incorporated in MSH particles, as indicated by TGA, was also observed by

340 Calabrese and co-workers (Calabrese et al., 2016), and similar trends have been presented with similar
341 nanocomposites (Liu et al., 2003).

342 The structure of individual montmorillonite layers was conserved in all the samples, as evident by the
343 combined (hk0) reflections obtained with PXRD. The (001) reflection shifted to a lower diffraction
344 angle for MSH particles as compared to untreated montmorillonite, which implied an increased
345 interlayer distance from 14.9 to 18.0 Å. This 3.1 Å increase agrees well with previous studies
346 (Calabrese et al., 2016; Calabrese et al., 2017). Under the assumption that the thickness of an
347 individual montmorillonite layer is 10 Å (Ploehn and Liu, 2006), the resulting distance between
348 individual montmorillonite layers was 8 Å, corresponding to 5-6 C-C alkane bonds (Skinner, 1945).
349 This distance indicated a relatively flat conformation of polysorbate 20, and effectively excluded the
350 possibility of micelle-like bilayer conformations or similar.

351 The (001) reflection was absent in digoxin-containing and lyophilised montmorillonite, which
352 implied exfoliation of montmorillonite layers as illustrated in Fig. 5. Furthermore, the appearance of
353 (002), (003), (005), and (006) and a narrower (001) reflection in the MSH particle diffractogram
354 suggested increased stacking order. Hence, lyophilisation of montmorillonite suspensions seems to
355 lead to exfoliation of individual layers. In contrast, when polysorbate 20 was introduced in the
356 preparation of MSH particles, which were subjected to the same lyophilisation cycle, montmorillonite
357 layers were not exfoliated. Instead, polysorbate 20 assisted in the stacking of montmorillonite layers
358 and increased the stacking order of montmorillonite layers.

359 The presence of the reflection at 29 ° for untreated montmorillonite and digoxin-treated
360 montmorillonite and the absence of the same reflection for MSH particles has not conclusively been
361 understood. The reflection could simply have been overshadowed in the diffractogram of MSH
362 particles.

363 Characterisation of MSH particles by SEM, PXRD, and TGA have proven a strong interaction
364 between polysorbate 20 and montmorillonite. Many different interactions between clays and organic
365 compounds have previously been described (Ruiz-Hitzky et al., 2010). Some of those are also
366 suggested here: i) ion-dipole interactions between oxyethylene (-CH₂-CH₂-O-) units of
367 polysorbate 20 and the negative surface charge of montmorillonite; ii) hydrogen bonding between
368 end hydroxyl groups of polysorbate 20 and the siloxane surface of montmorillonite.

369 4.2 Polysorbate 20-containing solutions modulated digoxin pharmacokinetics

370 The experimental design did not allow for thorough estimation of digoxin absorption rate constant
371 from the intestine, and for this reason, the first sampling point at 15 min was taken as a rough estimate
372 of absorption rate. Polysorbate 20 in the simple solution tended to increase C_{max} and C_{15 min} and
373 decreased t_{max}, which was also shown by Nielsen and co-workers in a previous study (Nielsen et al.,
374 2016). However, in contrast to this previous study, no change was observed in AUC_{0-6h} in the present
375 study. Overall, AUC-values were generally lower in the present study compared to the study by
376 Nielsen and co-workers. This may partly be caused by the inclusion of the AUC_{6-∞} part by Nielsen
377 and co-workers, which was not included in the present study. The less pronounced effect of
378 polysorbate 20 on digoxin pharmacokinetics may also partly be attributed to differences in
379 quantification methods and variation between animals and raw materials. Variation of the
380 composition between brands and lots of polysorbate 20 is well-documented (Hewitt et al., 2011),
381 which may influence the function of polysorbate 20 as a P-gp inhibitor. Furthermore, previous studies
382 on inhibition of intestinal transporters and carriers have also shown a clear modulation of the
383 pharmacokinetic profile and effects on C_{max} and t_{max}, but with no effects on AUC (Broberg et al.,
384 2012; Nohr et al., 2014). When preceding evidence is considered, the present study still indicates that
385 polysorbate 20 modulated the pharmacokinetics of digoxin, despite limited statistical strength. The

386 modulation of digoxin pharmacokinetics was ascribed to the inhibition of intestinal P-gp, leading to
387 lowered efflux, and increased intestinal absorption of digoxin.

388 4.3 *Montmorillonite-surfactant hybrid particles increased digoxin exposure*

389 When digoxin-containing montmorillonite was administered, the AUC_{0-6h} , C_{max} , and $C_{15\ min}$ decreased
390 compared to digoxin only, likely because of retention of digoxin by montmorillonite in the
391 formulation, which led to less digoxin available for absorption. This phenomenon has also been
392 observed by Dening and co-workers (Dening et al., 2018) when the lipophilic and cationic drug
393 substance, blonanserin, was intercalated into montmorillonite. Dening and co-workers investigated
394 blonanserin release from montmorillonite in a USP dissolution setup, where only 13 % was released
395 after 12 h. Accordingly, bioavailability in Sprague Dawley rats for montmorillonite-intercalated
396 blonanserin was reduced by 35 %, compared to the pure drug suspension (Dening et al., 2018). The
397 retention of digoxin in the present study showed that montmorillonite can also effectively adsorb
398 uncharged drug substances. Therefore, montmorillonite alone appeared to be unsuitable for
399 increasing oral digoxin absorption. Nevertheless, the lowering of digoxin exposure by
400 digoxin-containing montmorillonite was contrasted by the tendency of the MSH particles to increase
401 the exposure of digoxin. We therefore suggest that polysorbate 20 facilitated digoxin release from the
402 MSH particles and also inhibited P-gp activity, leading to an increased digoxin exposure. At present,
403 it was not possible to unequivocally distinguish these two effects from each other. Additionally, we
404 suggest that local co-release of digoxin and polysorbate 20 may have caused the observed increased
405 exposure by elevation of both polysorbate 20- and digoxin mucosal concentrations, compared to
406 polysorbate 20 and digoxin in simple solutions. However, neither the physicochemical
407 characterisation nor the *in vivo* performance of MSH particles have been able to confirm the
408 underlying mechanism, and further studies of the MSH particle-mucosa interaction are needed.

409 When the effects of MSH particles and digoxin-containing montmorillonite are compared,
410 montmorillonite exhibited a dual function with respect to digoxin retention and enhancement of P-gp
411 inhibition. This was observed as a decreased digoxin exposure for digoxin-containing
412 montmorillonite, relative to control, but also as an enhancement of digoxin exposure, when
413 montmorillonite was intercalated with polysorbate 20 in MSH particles. The observed effects of
414 digoxin-containing montmorillonite and MSH particles *in vivo* and the proposed mechanisms have
415 been illustrated in Fig. 5.

416 Clays and other solid carriers have also been applied to solidify LBFs, and some examples exists,
417 where the solidified LBF outperforms the liquid LBF *in vivo* (Denning et al., 2018; Tan et al., 2013) –
418 similarly to what have been observed in the present study. For example, a solidified silica-lipid hybrid
419 formulation of blonanserin tended to increase blonanserin AUC by 24 %, compared to a
420 corresponding medium-chain triglyceride solution (Denning et al., 2018).

421 In the present study, polysorbate 20 presented a dual function in MSH particles with the ability to
422 inhibit P-gp and to facilitate release of digoxin from montmorillonite surfaces. The facilitation of
423 drug release from montmorillonite by polysorbate 20 was also observed by Calabrese and co-workers
424 (Calabrese et al., 2017). 100 % release of the anionic compound, cinnamic acid, was achieved after
425 6 h from a montmorillonite-polysorbate 20 hybrid, whereas only 80 % was released from pure
426 montmorillonite (Calabrese et al., 2017).

427 Digoxin-containing montmorillonite retained digoxin and decreased digoxin exposure, while MSH
428 particles increased digoxin exposure. Therefore, changing the ratio between montmorillonite and
429 polysorbate 20 in future formulations may produce enhanced polysorbate 20-mediated P-gp
430 inhibition leading to increased P-gp substrate exposure.

431 **5 Conclusions**

432 The present study is the first to apply a surfactant-containing nanocomposite material to modulate an
433 intestinal efflux transporter, to our knowledge. Characterisation of MSH particles showed that
434 polysorbate 20 affected morphologic appearance of montmorillonite, was intercalated in the
435 interlayer spaces of montmorillonite, and that polysorbate 20 assisted in ordered stacking of
436 montmorillonite layers.

437 *In vivo*, MSH particles showed a tendency to increase digoxin exposure *via* P-gp inhibition, both
438 compared to digoxin administered alone and compared with co-administration of corresponding
439 polysorbate 20 doses in simple solutions. Furthermore, digoxin-containing montmorillonite, without
440 polysorbate 20, decreased digoxin exposure. This enhancement in digoxin exposure, when
441 administered as MSH particles, may be caused by mucosa-localised elevated concentrations of both
442 digoxin and polysorbate 20, which led to a more effective inhibition of P-gp. However, more research
443 is required to fully understand the underlying mechanism.

444 **6 Author information**

445 **Author contribution**

446 Conception and design of the study: RBN, AK, LD, KW, JS, UGN, RH, and CUN. Acquisition of
447 data: RBN and AK. Analysis and interpretation of data: RBN, AK, LD, KW, JS, UGN, RH, and CUN.
448 Drafting the article: RBN, UGN, RH, and CUN. Critical revising and final approval of the version
449 submitted: RBN, AK, LD, KW, JS, UGN, RH, and CUN.

450 **ORCID**

451 Rasmus Blaaholm Nielsen 0000-0003-1684-215X

452 Lieve Dillen 0000-0003-0573-9982

453 Jan Snoeys 0000-0003-3420-424X

454 Ulla Gro Nielsen 0000-0002-2336-3061

455 Carsten Uhd Nielsen 0000-0001-5776-6865

456 **Notes:** The authors declare no competing financial interests.

457 **7 Acknowledgements**

458 Researchers and technicians at Janssen R&D and The University of Southern Denmark, who helped
459 set up, conduct, and analyse various experiments, including Bjarke Strøm Larsen, Maria Læssøe
460 Pedersen, Nicholai Daugaard Jensen, Dorte Bomholdt Ravnsbæk, Tae-Hyun Kim, Dries
461 Versweyveld, Sanket Shah, Jasmine Bogaerts, Elene De Cleyn, Kore Van Mechelen, and Luc Sips
462 are hereby acknowledged.

463 The mobility action related to the project was financially supported by the Erasmus+ Programme,
464 Oticon Fonden, Knud Højgaards Fond, F.W. Frank og Hustru Angelina Franks Mindelegat, and
465 Henry og Mary Skovs Fond.

466

467 **8 References**

- 468 Aguzzi, C., Cerezo, P., Viseras, C., Caramella, C., 2007. Use of clays as drug delivery systems:
469 Possibilities and limitations. *Appl. Clay Sci.* 36, 22-36. <https://doi.org/10.1016/j.clay.2006.06.015>.
- 470 Al-Ali, A.A.A., Nielsen, R.B., Steffansen, B., Holm, R., Nielsen, C.U., 2019. Nonionic surfactants
471 modulate the transport activity of ATP-binding cassette (ABC) transporters and solute carriers
472 (SLC): Relevance to oral drug absorption. *Int. J. Pharm.* 566, 410-433.
473 <https://doi.org/10.1016/j.ijpharm.2019.05.033>.
- 474 Al-Ali, A.A.A., Quach, J.R.C., Bundgaard, C., Steffansen, B., Holm, R., Nielsen, C.U., 2018a.
475 Polysorbate 20 alters the oral bioavailability of etoposide in wild type and *mdr1a* deficient Sprague-
476 Dawley rats. *Int. J. Pharm.* 543, 352-360. <https://doi.org/10.1016/j.ijpharm.2018.04.006>.
- 477 Al-Ali, A.A.A., Steffansen, B., Holm, R., Nielsen, C.U., 2018b. Nonionic surfactants increase
478 digoxin absorption in Caco-2 and MDCKII MDR1 cells: Impact on P-glycoprotein inhibition,
479 barrier function, and repeated cellular exposure. *Int. J. Pharm.* 551, 270-280.
480 <https://doi.org/10.1016/j.ijpharm.2018.09.039>.
- 481 Al-Saraf, A., Holm, R., Nielsen, C.U., 2016. Tween 20 increases intestinal transport of doxorubicin
482 in vitro but not in vivo. *Int. J. Pharm.* 498, 66-69. <https://doi.org/10.1016/j.ijpharm.2015.12.017>.
- 483 Aranda, P., Ruiz-Hitzky, E., 1992. Poly(Ethylene Oxide)-Silicate Intercalation Materials. *Chem.*
484 *Mater.* 4, 1395-1403. <https://doi.org/10.1021/cm00024a048>.
- 485 Broberg, M.L., Holm, R., Tonsberg, H., Frolund, S., Ewon, K.B., Nielsen, A.L., Brodin, B., Jensen,
486 A., Kall, M.A., Christensen, K.V., Nielsen, C.U., 2012. Function and expression of the proton-
487 coupled amino acid transporter PAT1 along the rat gastrointestinal tract: implications for intestinal
488 absorption of gaboxadol. *Br. J. Pharmacol.* 167, 654-665. [https://doi.org/10.1111/j.1476-](https://doi.org/10.1111/j.1476-5381.2012.02030.x)
489 [5381.2012.02030.x](https://doi.org/10.1111/j.1476-5381.2012.02030.x).

490 Calabrese, I., Cavallaro, G., Lazzara, G., Merli, M., Sciascia, L., Liveri, M.L.T., 2016. Preparation
 491 and characterization of bio-organoclays using nonionic surfactant. *Adsorption* 22, 105-116.
 492 <https://doi.org/10.1007/s10450-015-9697-1>.

493 Calabrese, I., Cavallaro, G., Scialabba, C., Licciardi, M., Merli, M., Sciascia, L., Liveri, M.L.T.,
 494 2013. Montmorillonite nanodevices for the colon metronidazole delivery. *Int. J. Pharm.* 457, 224-
 495 236. <https://doi.org/10.1016/j.ijpharm.2013.09.017>.

496 Calabrese, I., Gelardi, G., Merli, M., Liveri, M.L.T., Sciascia, L., 2017. Clay-biosurfactant materials
 497 as functional drug delivery systems: Slowing down effect in the in vitro release of cinnamic acid.
 498 *Appl. Clay Sci.* 135, 567-574. <https://doi.org/10.1016/j.clay.2016.10.039>.

499 Cook, D., Brown, D., Alexander, R., March, R., Morgan, P., Satterthwaite, G., Pangalos, M.N.,
 500 2014. Lessons learned from the fate of AstraZeneca's drug pipeline: a five-dimensional framework.
 501 *Nat. Rev. Drug Discov.* 13, 419. <https://doi.org/10.1038/nrd4309>.

502 Cornaire, G., Woodley, J., Hermann, P., Cloarec, A., Arellano, U., Houin, G., 2004. Impact of
 503 excipients on the absorption of P-glycoprotein substrates in vitro and in vivo. *Int. J. Pharm.* 278,
 504 119-131. <https://doi.org/10.1016/j.ijpharm.2004.03.001>.

505 Dening, T.J., Rao, S., Thomas, N., Prestidge, C.A., 2017. Montmorillonite-lipid hybrid carriers for
 506 ionizable and neutral poorly water-soluble drugs: Formulation, characterization and in vitro
 507 lipolysis studies. *Int. J. Pharm.* 526, 95-105. <https://doi.org/10.1016/j.ijpharm.2017.04.063>.

508 Dening, T.J., Thomas, N., Rao, S., van Looveren, C., Cuyckens, F., Holm, R., Prestidge, C.A.,
 509 2018. Montmorillonite and Laponite Clay Materials for the Solidification of Lipid-Based
 510 Formulations for the Basic Drug Blonanserine: In Vitro and in Vivo Investigations. *Mol. Pharm.* 15,
 511 4148-4160. <https://doi.org/10.1021/acs.molpharmaceut.8b00555>.

512 Di, L., Kerns, E.H., 2016. Drug-Like Properties: Concepts, Structure Design and Methods from
 513 ADME to Toxicity Optimization, 2nd ed. Academic Press, Boston, USA.

514 Feeney, O.M., Crum, M.F., McEvoy, C.L., Trevaskis, N.L., Williams, H.D., Pouton, C.W.,
 515 Charman, W.N., Bergstrom, C.A.S., Porter, C.J.H., 2016. 50 years of oral lipid-based formulations:
 516 Provenance, progress and future perspectives. *Adv. Drug Deliv. Rev.* 101, 167-194.
 517 <https://doi.org/10.1016/j.addr.2016.04.007>.

518 Gurjar, R., Chan, C.Y.S., Curley, P., Sharp, J., Chiong, J., Rannard, S., Siccardi, M., Owen, A.,
 519 2018. Inhibitory Effects of Commonly Used Excipients on P-Glycoprotein in Vitro. *Mol. Pharm.*
 520 15, 4835-4842. <https://doi.org/10.1021/acs.molpharmaceut.8b00482>.

521 Hensen, E.J.M., Smit, B., 2002. Why Clays Swell. *J. Phys. Chem. B* 106, 12664-12667.
 522 <https://doi.org/10.1021/jp0264883>.

523 Hewitt, D., Alvarez, M., Robinson, K., Ji, J.Y., Wang, Y.J., Kao, Y.H., Zhang, T., 2011. Mixed-
 524 mode and reversed-phase liquid chromatography-tandem mass spectrometry methodologies to study
 525 composition and base hydrolysis of polysorbate 20 and 80. *J. Chromatogr. A* 1218, 2138-2145.
 526 <https://doi.org/10.1016/j.chroma.2010.09.057>.

527 Iannuccelli, V., Maretti, E., Montorsi, M., Rustichelli, C., Sacchetti, F., Leo, E., 2015.
 528 Gastroretentive montmorillonite-tetracycline nanoclay for the treatment of *Helicobacter pylori*
 529 infection. *Int. J. Pharm.* 493, 295-304. <https://doi.org/10.1016/j.ijpharm.2015.06.049>.

530 Kokabi, M., Sirousazar, M., Hassan, Z.M., 2007. PVA-clay nanocomposite hydrogels for wound
 531 dressing. *Eur. Polym. J.* 43, 773-781. <https://doi.org/10.1016/j.eurpolymj.2006.11.030>.

532 Kola, I., Landis, J., 2004. Can the pharmaceutical industry reduce attrition rates? *Nat. Rev. Drug*
 533 *Discov.* 3, 711-715. <https://doi.org/10.1038/nrd1470>.

534 Leslie, E.M., Deeley, R.G., Cole, S.P.C., 2005. Multidrug resistance proteins: role of P-
 535 glycoprotein, MRP1, MRP2, and BCRP (ABCG2) in tissue defense. *Toxicol. Appl. Pharmacol.*
 536 204, 216-237. <https://doi.org/10.1016/j.taap.2004.10.012>.
 537 Lin, J.H., Yamazaki, M., 2003. Role of P-glycoprotein in pharmacokinetics - Clinical implications.
 538 *Clin. Pharmacokinet.* 42, 59-98. <https://doi.org/10.2165/00003088-200342010-00003>.
 539 Liu, T.X., Lim, K.P., Tjiu, W.C., Pramoda, K.P., Chen, Z.K., 2003. Preparation and characterization
 540 of nylon 11/organoclay nanocomposites. *Polymer* 44, 3529-3535. [https://doi.org/10.1016/s0032-](https://doi.org/10.1016/s0032-3861(03)00252-0)
 541 [3861\(03\)00252-0](https://doi.org/10.1016/s0032-3861(03)00252-0).
 542 Lo, Y.I., 2003. Relationships between the hydrophilic-lipophilic balance values of pharmaceutical
 543 excipients and their multidrug resistance modulating effect in Caco-2 cells and rat intestines. *J.*
 544 *Control. Release* 90, 37-48. [https://doi.org/10.1016/S0168-3659\(03\)00163-9](https://doi.org/10.1016/S0168-3659(03)00163-9).
 545 Nair, A.B., Jacob, S., 2016. A simple practice guide for dose conversion between animals and
 546 human. *J. Basic Clin. Pharm.* 7, 27-31. <https://doi.org/10.4103/0976-0105.177703>.
 547 Nielsen, C.U., Abdulhussein, A.A., Colak, D., Holm, R., 2016. Polysorbate 20 increases oral
 548 absorption of digoxin in wild-type Sprague Dawley rats, but not in mdr1a(-/-) Sprague Dawley rats.
 549 *Int. J. Pharm.* 513, 78-87. <https://doi.org/10.1016/j.ijpharm.2016.09.011>.
 550 Nohr, M.K., Thale, Z.I., Brodin, B., Hansen, S.H., Holm, R., Nielsen, C.U., 2014. Intestinal
 551 absorption of the antiepileptic drug substance vigabatrin is altered by infant formula in vitro and in
 552 vivo. *Pharmacol. Res. Perspect.* 2, e00036. <https://doi.org/10.1002/prp2.36>.
 553 Onnainty, R., Onida, B., Paez, P., Longhi, M., Barresi, A., Granero, G., 2016. Targeted chitosan-
 554 based bionanocomposites for controlled oral mucosal delivery of chlorhexidine. *Int. J. Pharm.* 509,
 555 408-418. <https://doi.org/10.1016/j.ijpharm.2016.06.011>.

556 Ploehn, H.J., Liu, C., 2006. Quantitative Analysis of Montmorillonite Platelet Size by Atomic Force
 557 Microscopy. *Ind. Eng. Chem. Res.* 45, 7025-7034. <https://doi.org/10.1021/ie051392r>.
 558 Rhim, J.W., Park, H.M., Ha, C.S., 2013. Bio-nanocomposites for food packaging applications.
 559 *Prog. Polym. Sci.* 38, 1629-1652. <https://doi.org/10.1016/j.progpolymsci.2013.05.008>.
 560 Ruiz-Hitzky, E., Aranda, P., Darder, M., Rytwo, G., 2010. Hybrid materials based on clays for
 561 environmental and biomedical applications. *J. Mater. Chem.* 20, 9306-9321.
 562 <https://doi.org/10.1039/c0jm00432d>.
 563 Sheskey, P.J., Cook, W.G., Cable, C.G., 2017. *Handbook of Pharmaceutical Excipients*, 8th ed.
 564 Pharmaceutical Press, London, UK.
 565 Skinner, H.A., 1945. A revision of some bond-energy values and the variation of bond-energy with
 566 bond-length. *Trans. Faraday Soc.* 41, 645-662. <https://doi.org/10.1039/tf9454100645>.
 567 Su, K.S.E., Carstensen, J.T., 1972. Nature of bonding in montmorillonite adsorbates II: Bonding as
 568 an ion-dipole interaction. *J. Pharm. Sci.* 61, 420-424. <https://doi.org/10.1002/jps.2600610321>.
 569 Tan, A., Rao, S., Prestidge, C.A., 2013. Transforming Lipid-Based Oral Drug Delivery Systems
 570 into Solid Dosage Forms: An Overview of Solid Carriers, Physicochemical Properties, and
 571 Biopharmaceutical Performance. *Pharm. Res.* 30, 2993-3017. [https://doi.org/10.1007/s11095-013-](https://doi.org/10.1007/s11095-013-1107-3)
 572 [1107-3](https://doi.org/10.1007/s11095-013-1107-3).
 573 Thiebaut, F., Tsuruo, T., Hamada, H., Gottesman, M.M., Pastan, I., Willingham, M.C., 1987.
 574 Cellular localization of the multidrug-resistance gene product P-glycoprotein in normal human
 575 tissues. *Proc. Natl. Acad. Sci. U.S.A.* 84, 7735-7738. <https://doi.org/10.1073/pnas.84.21.7735>.
 576 Viani, A., Gaultieri, A.F., Artioli, G., 2002. The nature of disorder in montmorillonite by simulation
 577 of X-ray powder patterns. *Am. Mineral.* 87, 966-975. <https://doi.org/10.2138/am-2002-0720>.

578 Wang, L., Wang, A.Q., 2007. Adsorption characteristics of Congo Red onto the
579 chitelsan/montmorillonite nanocomposite. J. Hazard. Mater. 147, 979-985.
580 <https://doi.org/10.1016/j.jhazmat.2007.01.145>.

581 Zhang, H.J., Yao, M., Morrison, R.A., Chong, S.H., 2003. Commonly used surfactant, tween 80,
582 improves absorption of P-glycoprotein substrate, digoxin, in rats. Arch. Pharmacol Res. 26, 768-
583 772. <https://doi.org/10.1007/bf02976689>.

584

585

586 9 Figure Legends

587 **Fig. 1:** Representative scanning electron microscopy images of A) Untreated montmorillonite, B)
588 digoxin-containing montmorillonite, C) montmorillonite-surfactant hybrid (MSH) particles
589 formulation A, and D) MSH E. $\times 8700$ magnification. Scaling bar = 10 μm .

590 **Fig. 2:** Representative runs of thermogravimetric analysis of 2-4 mg aliquots of untreated
591 montmorillonite (MMT), lyophilised montmorillonite (Lyo-MMT), digoxin-containing
592 montmorillonite (DG-MMT), montmorillonite-surfactant hybrid particles (MSH), and polysorbate 20
593 (PS20). Equilibrated at 30 $^{\circ}\text{C}$, heated to 700 $^{\circ}\text{C}$ at a rate of 10 $^{\circ}\text{C min}^{-1}$.

594 **Fig. 3:** X-ray diffractograms and *hkl*-indexing of untreated montmorillonite (MMT), lyophilised
595 montmorillonite (Lyo-MMT), digoxin-containing montmorillonite (DG-MMT), and
596 montmorillonite-surfactant hybrid particles (MSH) formulation A (representative of all MSH
597 formulations). Stacked diffractograms, dotted lines represent 0 for each one. Insert: Magnification of
598 3-8 $^{\circ}$. Cu K_{α} radiation source ($\lambda = 1.5406 \text{ \AA}$) over the range of 3-50 $^{\circ}2\theta$ with a scan speed of 0.254 $^{\circ}$
599 s^{-1} and a step size of 0.0167 $^{\circ}$. Intensity in arbitrary units (a.u.).

600 **Fig. 4:** Time-concentration profiles of digoxin after oral administration of 0.2 mg kg^{-1} digoxin to
601 fasted male Sprague Dawley rats (245-300 g) as solutions or suspensions in 40 % v/v ethanol in water.
602 Comparisons of A) digoxin administered alone in solution, with co-administration of 55, 274, or 548
603 mg kg^{-1} polysorbate 20 (PS20), B) as digoxin-containing montmorillonite (DG-MMT, 548 mg kg^{-1}
604 MMT) or as montmorillonite-surfactant hybrid (MSH) particles containing 55-137 mg kg^{-1}
605 polysorbate 20 (PS20) and 55-137 mg kg^{-1} montmorillonite (MMT) in a 1:1 ratio, and C) as
606 montmorillonite-surfactant hybrid (MSH) particles containing 274-548 mg kg^{-1} MMT and 274-548
607 mg kg^{-1} PS20 in a 1:1 ratio. D) is an additional representation of selected formulations for direct

608 comparison. Values are given as mean \pm SEM, n=6. All lines are simple connecting lines for
609 overview.

610 **Fig. 5.** Illustration of the observed effects of the treatment of montmorillonite with digoxin (blue) or
611 digoxin and polysorbate 20 (red) prior to lyophilisation to form digoxin-containing montmorillonite
612 and montmorillonite-surfactant hybrid (MSH) particles, respectively. Digoxin-containing
613 montmorillonite is exfoliated (no stacking order), and MSH particles elicit increased stacking order
614 and an increase of interlayer distance from 14.9 Å in untreated montmorillonite to 18.0 Å. Overview
615 of the observed effects *in vivo* after oral administration of digoxin-containing montmorillonite and
616 montmorillonite-surfactant hybrid (MSH) particles.

617 **Fig. S1:** Scanning electron microscopy images of A) Untreated montmorillonite, B) digoxin-
618 containing montmorillonite, C) montmorillonite-surfactant hybrid (MSH) particles formulation A and
619 D), MSH E. $\times 430$ magnification. Scaling bar = 200 μm .

620 **Fig. S2:** Scanning electron microscopy images of lyophilised montmorillonite. A) $\times 430$ and B) $\times 8700$
621 magnification. Scaling bars = 10 and 200 μm respectively.

622 **Table 1.**

623 **Table 2.**

624 **Table 3.**

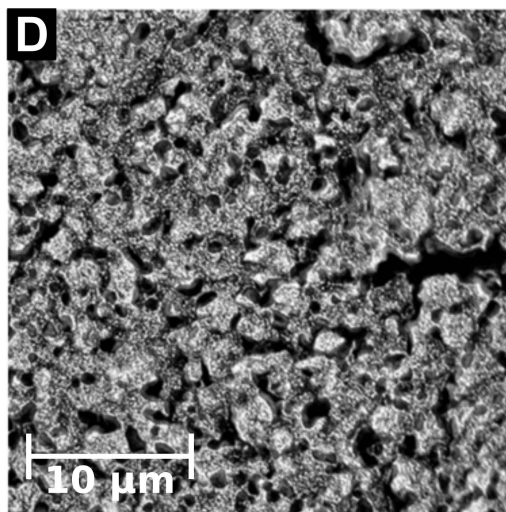
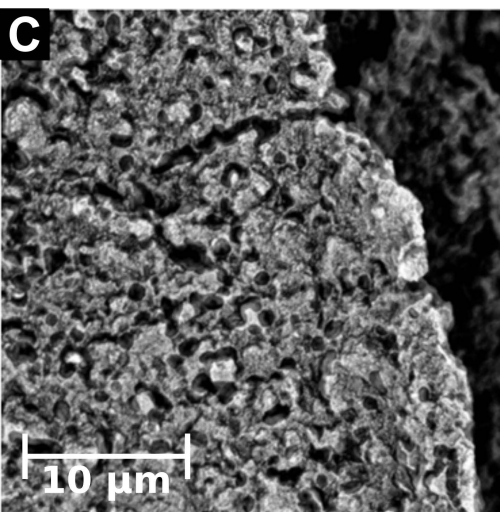
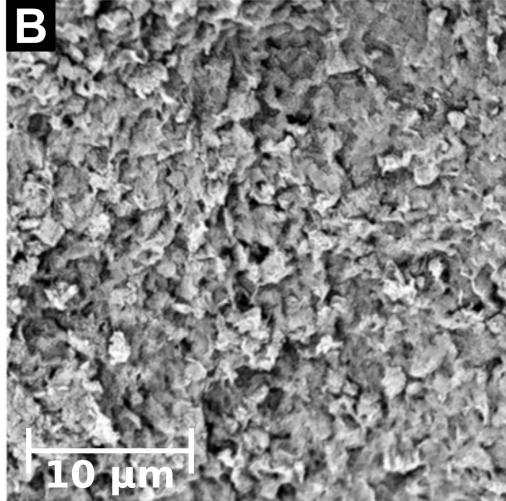
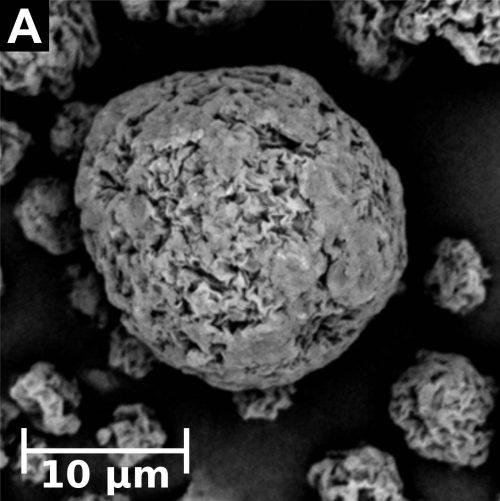
625 **Table S1.**

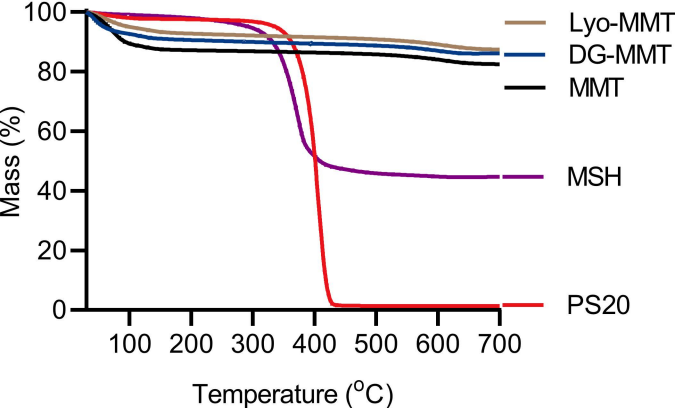
626 **10 Supplementary Material**

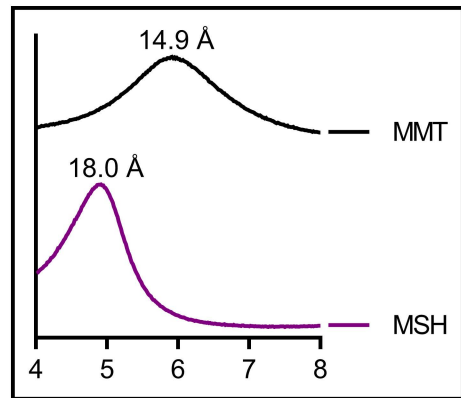
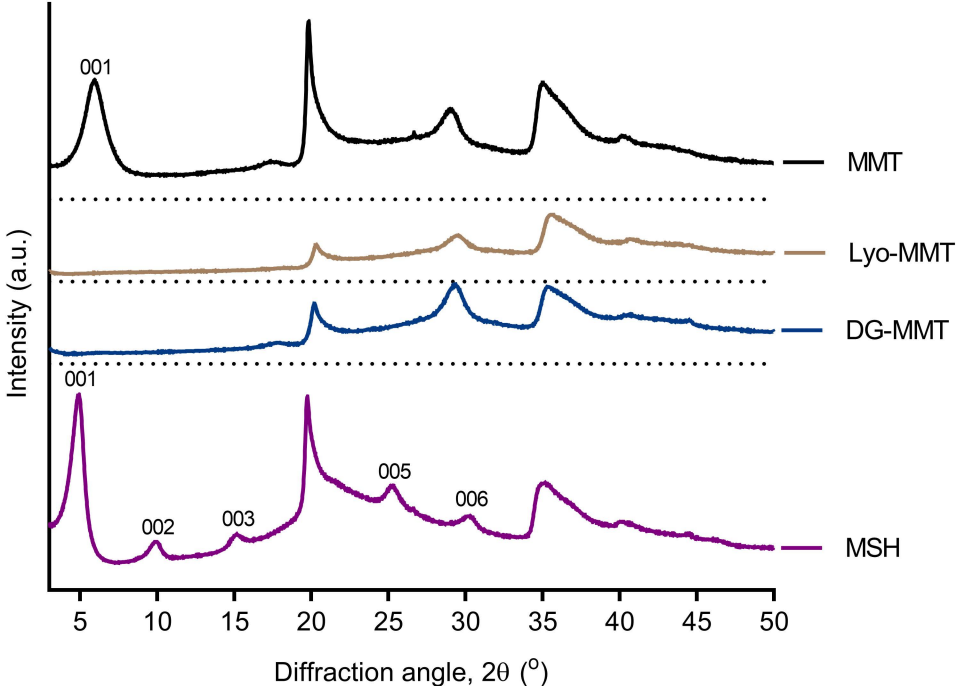
627 *Fig. S1*

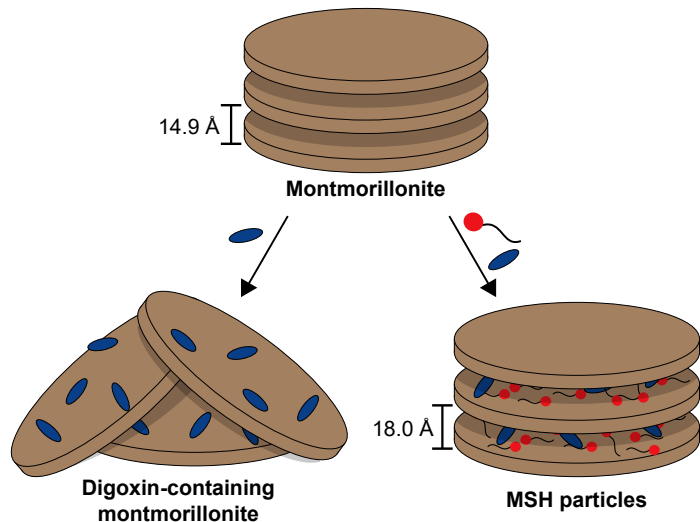
628 *Fig. S2*

629 *Table S1*









Digoxin adsorption to montmorillonite

Intestinal digoxin absorption

P-gp inhibition

Retention of digoxin by montmorillonite

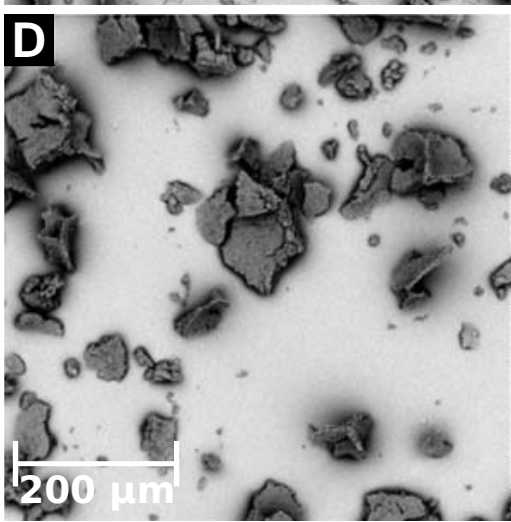
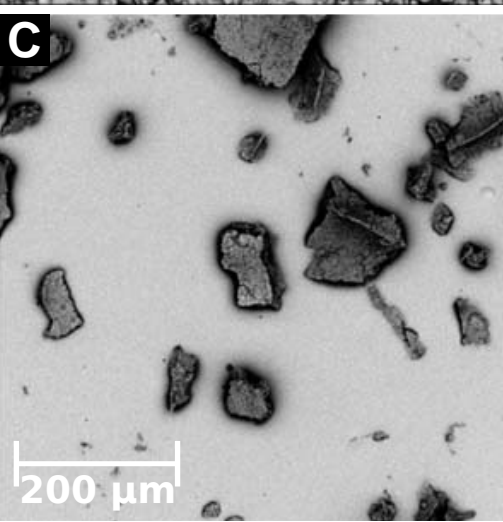
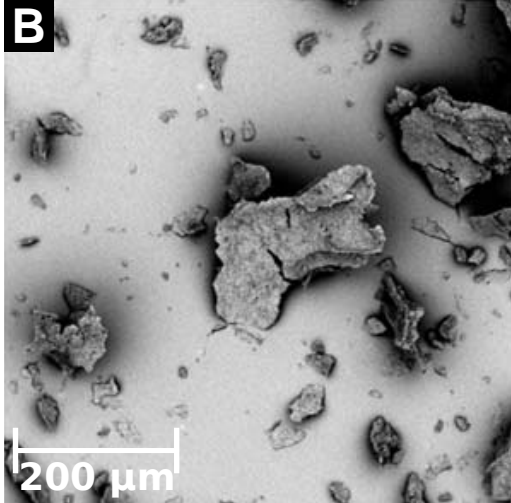
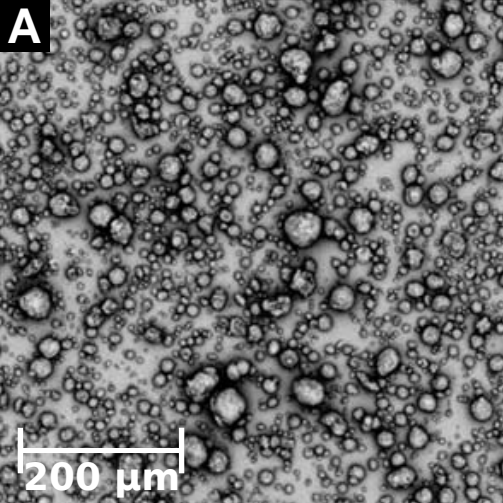
Lowered amount available for absorption

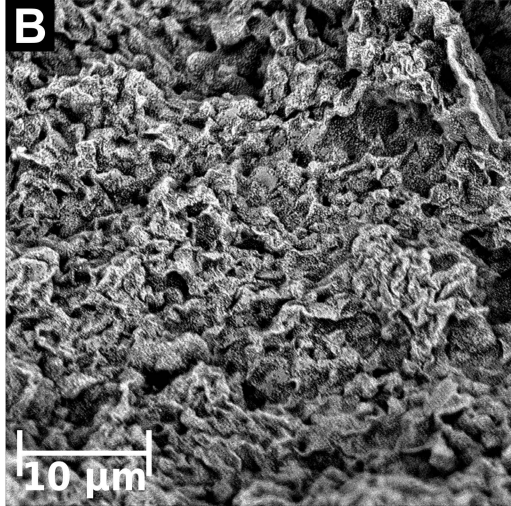
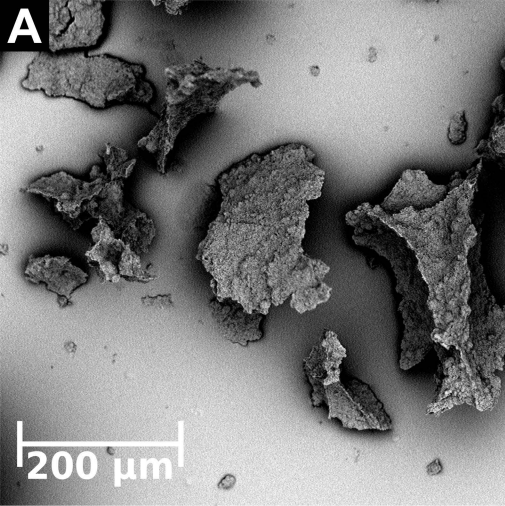
No effect

Digoxin release facilitated by polysorbate 20

Increased absorption

Enhanced polysorbate 20-mediated P-gp inhibition by local co-release







Montmorillonite



Digoxin



Digoxin +
Polysorbate 20

+ Digoxin

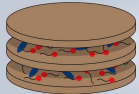


Digoxin-containing
montmorillonite

+ Digoxin



Polysorbate 20



Montmorillonite-
surfactant hybrid

C_{max} after
oral adm.



Table 1. Overview of prepared formulations

The prepared formulations including the added amounts of montmorillonite, polysorbate 20, and digoxin as well as the calculated final content of these (% w/w).

Formulation	Amount added (mg)			Final content (% w/w)		
	Montmorillonite	Polysorbate 20	Digoxin	Montmorillonite	Polysorbate 20	Digoxin
MSH A	2739	2750	1.00	50	50	0.018
MSH B	2052	2051	1.00	50	50	0.024
MSH C	1368	1372	1.00	50	50	0.036
MSH D	679	689	1.00	50	50	0.073
MSH E	273	275	1.00	50	50	0.182
Lyophilised montmorillonite	2738	-	-	100	-	-
Digoxin-containing montmorillonite	2738	-	1.00	100	-	0.037

MSH, montmorillonite-surfactant hybrid

Table 2. *In vivo* study overview

Overview of administered dose of polysorbate 20, montmorillonite, and digoxin along with the amount of polysorbate 20 in the dosing formulation (% v/v) for each group of male Sprague Dawley rats.

Group number	1	2	3	4	5	6	7	8	9	10
Formulation	Solution				Digoxin-containing montmorillonite suspension	MSH particle suspension				
Polysorbate 20 in dosing formulation (% v/v)	-	1	5	10	-	1	2.5	5	7.5	10
Digoxin dose (mg kg ⁻¹)	0.2	0.2	0.2	0.2	0.2	0.2	0.2	0.2	0.2	0.2
Polysorbate 20 dose (mg kg ⁻¹)	-	55	274	548	-	55	137	274	411	548
Montmorillonite dose (mg kg ⁻¹)	-	-	-	-	548	55	137	274	411	548

MSH, montmorillonite-surfactant hybrid

Table 3. Estimated pharmacokinetic parameters.

Formulation	AUC _{0-6h} ± SEM (µg min mL ⁻¹)	C _{max} ± SEM (ng mL ⁻¹)	C _{15 min} ± SEM (ng mL ⁻¹)	t _{max} [Q1;Q3] (min)	t _{1/2} ± SEM (h)
Digoxin	6.05 ± 0.86	29.6 ± 4.9	21.8 ± 1.5	45 [30;60]	2.27 ± 0.15
+ 55 mg kg⁻¹ polysorbate 20	6.07 ± 0.46	43.8 ± 4.1	37.9 ± 4.6*	22.5 [15;48.8]	1.76 ± 0.18
+ 274 mg kg⁻¹ polysorbate 20	5.75 ± 0.75	41.1 ± 4.0	35.6 ± 3.1*	22.5 [15;33.8]	1.84 ± 0.16
+ 548 mg kg⁻¹ polysorbate 20	6.19 ± 0.63	42.6 ± 6.9	34.5 ± 4.2	30 [15;45]	2.42 ± 0.16
Digoxin-containing montmorillonite (548 mg kg⁻¹ montmorillonite)	2.78 ± 0.21*	14.1 ± 0.9*	12.6 ± 1.2*	37.5 [15;48.8]	2.78 ± 0.34
MSH (55 mg kg⁻¹ montmorillonite & polysorbate 20)	5.14 ± 0.34 [#]	33.0 ± 2.4	27.9 ± 3.5	30 [15;45]	2.46 ± 0.25
MSH (137 mg kg⁻¹ montmorillonite & polysorbate 20)	6.81 ± 0.59 [#]	51.2 ± 8.0 [#]	37.3 ± 4.3 [#]	37.5 [30;45]	2.54 ± 0.36
MSH (274 mg kg⁻¹ montmorillonite & polysorbate 20)	6.58 ± 0.66 [#]	50.8 ± 7.5 [#]	49.9 ± 7.9* [#]	15 [15;22.5]	1.99 ± 0.15
MSH (411 mg kg⁻¹ montmorillonite & polysorbate 20)	7.71 ± 0.88 [#]	46.7 ± 8.5 [#]	38.6 ± 6.1 [#]	37.5 [15;48.8]	2.30 ± 0.19
MSH (548 mg kg⁻¹ montmorillonite & polysorbate 20)	7.94 ± 0.66 [#]	56.4 ± 9.0* [#]	41.1 ± 4.5* [#]	30 [30;45]	1.94 ± 0.08

C_{15 min}, the plasma concentration at the first sampling point (15 min); MSH, montmorillonite-surfactant hybrid particles. t_{max} is given as median [25th percentile;75th percentile]. Significantly different from digoxin only marked by * and significantly different from digoxin-containing montmorillonite marked by [#] (p < 0.05).

Table S1. Thermogravimetric mass loss of applied formulations by temperature intervals.

Formulation	Mass lost (%) in temp. interval				
	30 - 100 °C	100 - 160 °C	160 - 500 °C	500 - 700 °C	700 °C
	Evap. adsorbed water	Evap. interlayer water	Evap. interlayer water + polysorbate 20 decomp.	Montmorillonite dehydroxylation	Residual
Untreated montmorillonite	10.6	2.0	1.6	3.3	82.5
Lyophilised montmorillonite	5.0	1.9	2.3	3.4	87.4
Digoxin-containing montmorillonite	7.4	1.7	2.2	2.6	86.1
Polysorbate 20	2.0	0.3	96.3	0.0	1.4
MSH particles	0.9	0.5	52.7	1.2	44.7

MSH, montmorillonite-surfactant hybrid. The defined intervals were ascribed to evaporation (evap.) of adsorbed water, interlayer water, polysorbate 20 decomposition (decomp.), and montmorillonite dehydroxylation.